Int. J. Solids Structures Vol. 18, No. 11, pp. 989–1005, 1982
Printed in Great Britain.

0020-7683/82/110989-17$03.00/0
Pergamon Press Ltd.

AN EXAMINATION OF FOUR VISCOPLASTIC CONSTITUTIVE THEORIES IN UNIAXIAL MONOTONIC LOADING

E. P. CERNOCKY
Department of Mechanical Engineering, University of Colorado, Boulder, CO 80309, U.S.A.

(*Received* 3 *August* 1981)

Abstract—The predictions of four constitutive theories of viscoplasticity are examined and compared in uniaxial homogeneous deformations. Each theory is fitted to the same stress–strain data, and both analytical and numerical methods are employed to highlight similarities and differences between their predictions.

Asymptotic limits are given which represent steady-state behavior of the solutions, and the limits are used to provide analytical methods for fitting test data. Different manifestations of strain-rate and stress-rate history effects predicted by the theories are compared, and the theories are shown to share a significant qualitative bias between responses to stress- and strain-controlled loading.

INTRODUCTION

The demands of an evolving technology and the advent of powerful computational software have encouraged the continuing development of constitutive equations of inelastic metal behavior. Development of constitutive theories has found increasing support from concurrent experiments indicating significant rate-dependence of metal behavior at low, room, and elevated temperatures. Such rate-dependence is manifested in rate-sensitivity of the yield stress and the flow stress[1–23], in creep and relaxation behavior[1–3, 24–30], and in the wavespeeds of propagating plastic waves[31–36]. Various viscoplastic constitutive theories have been developed in order to represent different facets of the rate- and history-dependent behavior observed in such experiments, and these theories use different respositories for modeling inelastic behavior.

In some cases[37–39] the constitutive equations are nonlinear in the strain-rate while in other cases[40–47] the equations are linear in the strain-rate and nonlinear in stress or strain. Some theories[48–53] are motivated by material science while other theories[37–47, 54–56] are primarily phenomenological in their foundations. In the viscoplastic endochronic theory[38, 39] a non-decreasing and rate-dependent parameter is employed to model both rate-dependence and material-memory for the prior plastic deformation. Alternatively the theory proposed by Bodner and Partom[45] uses a flow law which depends on the plastic work. Yet another approach[12, 41–44, 55] proposes that the plastic strain-rate depends on the difference between the flow stress and the corresponding value of an equilibrium stress–strain curve evaluated at the same strain.

Because different theories use different repositories for modeling rate-dependence and memory for plastic deformation, they predict subtly different manifestations of inelastic behavior. Here the predictions of four visco-plastic theories are examined and compared in uniaxial homogeneous deformations. Each theory is shown to predict qualitative biases between responses to stress- and strain-controlled loading. Asymptotic limits are obtained which characterize steady-state stress–strain behavior and which are useful in fitting the models to experimental data.

We examine theories presented by Bodner and Partom[45], Cernocky and Krempl[43, 44], and Lin and Wu[38]. In addition a new version of the endochronic theory of Wu and Yip[39] is proposed and examined. These theories share a capability of modeling nonlinear rate-dependence of stress–strain behavior, and in the forms presented here each theory models material behavior as inelastic at all times; no yields surfaces are used. Additional viscoplastic theories are available, and it is only for practicality that this study is limited to four theories.

Material constants are determined by fitting each model to the same constant strain-rate stress–strain data suggested by the quasi-static experiments of Krempl[1] and the dynamic experiments of Albertini and Montagnani[5]; see Table 1. The initial elastic slope is prescribed,

Table 1. Stress–strain data and responses at 1% strain

Strain-Rate (s^{-1})	10^{-8}	10^{-5}	10^{-3}	10^{-2}	69	177	808
Experimental Stress (Ksi)	22.3	26.2	29.3	32.0	42.8	46.0	52.3
Stress from Model I (Ksi)	22.2	26.2	29.8	31.9	44.1	46.0	49.3
Stress from Model II (Ksi)	22.4	26.2	29.9	32.2	44.3	46.0	48.8
Stress from Model III (Ksi)	22.5	26.2	29.5	31.6	43.9	45.9	49.5
Stress from Model IV (Ksi)	22.5	26.2	29.5	31.6	44.0	46.0	49.7

Models I–IV are fitted to data for 304 Stainless Steel at 1% strain for the strain-rates 10^{-5} s^{-1} and 177 s^{-1}. Data for strain-rates below 10^{-2} s^{-1} is obtained from [1], and data for rates above 10^{-2} s^{-1} corresponds to [5]. The cold worked data from [5] has been shifted to match the annealed data from [1] at the strain-rate 10^{-2} s^{-1} in order to approximate dynamic responses of the annealed material. The responses of Models I–IV are obtained through numerical solutions of the constitutive equations.

and each model is fitted to two stress–strain data points at 1% strain using the limits developed here. The data points are arbitrarily selected to correspond to the strain-rates $10^{-5}\,s^{-1}$ and $177\,s^{-1}$. We also specify the stress–strain slope at the lower (static-rate) data point. Additional data points may be fitted by using the limits to obtain systems of equations which are numerically solved for unknown constants. This case is not pursued here because our interest is comparison of the qualitative behavior of the models rather than curve-fitting quantitative responses.

THE CONSTITUTIVE EQUATIONS

We designate σ and ϵ as the axial stress and infinitesimal strain, respectively; ϵ_{pl} is the corresponding *rate-dependent* plastic strain. The theory of Bodner and Partom [45] is arbitrarily designed as Model I, and the flow law is†

$$\dot{\epsilon}_{pl} = a_0 \exp\left[-(F[W_{pl}]/|\sigma|)^{b_0}\right] \operatorname{sign}[\sigma]. \tag{1}$$

A superimposed dot indicates differentation with respect to time, and square brackets denote functions of the indicated arguments. Sign[σ] equals ± 1 corresponding to positive and negative stress, and W_{pl} is the plastic work. $F[\ ]$ is a bounded, increasing function, and a_0, b_0 are positive constants.

For reference Model II denotes the constitutive equation from [43, 44] with the flow law

$$\dot{\epsilon}_{pl} = \frac{\sigma - g[\epsilon]}{E\,k[\sigma - g[\epsilon]]}. \tag{2}$$

In (2) E is the constant elastic modulus. The function $g[\ ]$ represents an equilibrium stress–strain response of the material, and it has the appearance of a tensile/compressive stress–strain curve [43, 57]. The initial slope of $g[\ ]$ is E, and for convenience and simplicity we take the slope at large strain to be the constant E_t. The difference between the flow stress and equilibrium response is referred to as the overstress, and $k[\ ]$ is a positive decreasing function of $|\sigma - g|$ given in the Appendix.

The rate-dependent endochronic theory of Lin and Wu [38] is designated as Model III, and

†An alternative finite-deformation representation of Model I is also presented in [45].

its flow law is

$$\dot{\epsilon}_{p1} = \frac{c_0 \dot{\zeta} \sigma}{E(1 + d_0 \zeta)} \tag{3}$$

where

$$\dot{\zeta} = K[\dot{\epsilon}]|\dot{\epsilon}|. \tag{4}$$

Here $K[\ ]$ is a nonlinear function of the strain-rate magnitude given in [38], and ζ is the rate-dependent "endochronic time"; c_0 and d_0 are material constants.

In an alternative endochronic theory Wu and Yip[39] replaced the total strain-rate in (4) with the plastic strain-rate, and they replaced (3) with a different flow law. Their theory uses a yield surface while Models I–III do not use yield surfaces. Further the principal advantage of the original endochronic theories[61, 38] was their freedom from yield surfaces.

Here we propose a new version of the rate-dependent endochronic theory by replacing the total strain-rate in (4) with the plastic strain-rate as in [39], but *without* using yield surfaces. We replace (4) with

$$\dot{\zeta} = K[\dot{\epsilon}_{p1}]|\dot{\epsilon}_{p1}| \tag{5}$$

but we keep the flow law (3), using the endochronic time from (5).

Substitution of (5) into (3) results in an implicit flow law for Model IV

$$K[\dot{\epsilon}_{p1}] = \frac{E(1 + d_0 \zeta)}{c_0 |\sigma|}. \tag{6}$$

In (5) and (6) $K[\ ]$ may be any positive decreasing function of the plastic strain-rate such that $K[\ ]\dot{\epsilon}_{p1}$ vanishes when $\dot{\epsilon}_{p1} = 0$. The flow law (6) applies at all times and behavior is always inelastic.

In this study we use the particular representation of $K[\ ]$ proposed in [38, 39]

$$K[\dot{\epsilon}_{p1}] = K_0 - K_1 \log_e[K_2 |\dot{\epsilon}_{p1}|]. \tag{7}$$

For the case of Model III the plastic strain-rate in (7) is replaced by the total strain-rate. For this particular representation of $K[\ ]$ the flow law of Model IV may be rewritten as

$$\dot{\epsilon}_{p1} = A_0 \exp\left[-\frac{E(1 + d_0 \zeta)}{c_0 B_0 |\sigma|} \right] \text{sign}[\sigma]. \tag{8}$$

The constants A_0, B_0 are related to constants in $K[\ ]$; see the Appendix.

LIMITING BEHAVIOR AT LARGE TIME

Constant strain-rate loading

In order to identify the large-time stress–strain behavior predicted by the models we formally determine limits of their responses as time and strain go to infinity in constant strain-rate, tensile loading. These limits become approximately satisfied at small stress and strain and characterize a *steady-state* facet of stress–strain behavior. To obtain the limits we use integral-equation representations of the constitutive equations. The same limits may also be obtained by requiring that $\ddot{\epsilon}_{p1}$ vanish at infinite strain (time).

Because the stress from Model II grows unbounded with infinite time, we examine the infinite-time limit of the overstress. The limits of integral equations for the overstress and for the stress-rate[43] produce

$$\{\sigma - g\} = (E - E_t)\dot{\epsilon}\, k[\{\sigma - g\}] \tag{9}$$

and

$$\left\{\frac{d\sigma}{d\epsilon}\right\} = E_t. \tag{10}$$

Here braces { } denote the value of their argument at infinite time. These limits indicate that the growth of stress at large time parallels the growth of $g[\ ]$, and that the overstress approaches a finite bound which depends nonlinearly on the strain-rate. At large time the stress–strain slope equals the constant E_t for any strain-rate (Fig. 3).

For Model I we rewrite the constitutive equation as an integral equation

$$\sigma = \int_0^t E\dot{\epsilon} \exp\left[-\int_0^t H[s]\,ds\right] d\tau \tag{11}$$

where

$$H[s] = \frac{E.a_0}{\sigma[s]} \exp\left[-\left(\frac{F[W_{p1}[s]]}{\sigma[s]}\right)^{b_0}\right]. \tag{12}$$

The infinite-time limit of (11) results in the limits for the stress response

$$\{\sigma\} = F[\infty]\,(\log_e[a_0/\dot{\epsilon}])^{-1/b_0} \tag{13}$$

and

$$\left\{\frac{d\sigma}{d\epsilon}\right\} = 0. \tag{14}$$

In (13) $F[\ ]$ is evaluated at $W_{p1} = \infty$, and $F[\ ]$ is a bounded function. The limits indicate that as strain (time) grows infinite in constant strain-rate loading, the stress approaches a finite bound which depends nonlinearly on the strain-rate, and the slope vanishes.

For both models III and IV the stress-rates may be written as

$$\dot{\sigma} = E\dot{\epsilon} - c_0\dot{\zeta}(1 + d_0\zeta[t])^{-(c_0/d_0+1)} \int_0^t E\dot{\epsilon}(1 + d_0\zeta[\tau])^{c_0/d_0}\,d\tau. \tag{15}$$

In (15) ζ and $\dot{\zeta}$ correspond to (4) or (5) for the respective cases of Models III and IV. From the limit of (15) we obtain

$$\left\{\frac{d\sigma}{d\epsilon}\right\} = \frac{E\,d_0}{c_0 + d_0}. \tag{16}$$

The limit (16) is the same for Models III and IV despite the different definitions of endochronic time and the different arguments in $K[\ ]$ for these models. From (16) the responses of Models III and IV eventually have the same constant slope for all strain-rates (Figs. 5 and 6).

Substitution of (16) into (3) and (4) results in the infinite-time limit for the response of Model III

$$\{\sigma - U[\zeta, \dot{\epsilon}]\} = \frac{E}{(c_0 + d_0)\,K[\dot{\epsilon}]} \tag{17}$$

where

$$U[\zeta, \dot{\epsilon}] = \frac{E\,d_0\,\zeta}{(c_0 + d_0)\,K[\dot{\epsilon}]}. \tag{18}$$

Here $\zeta = K[\dot{\epsilon}]\epsilon$ for *constant* strain-rate loading. At large time the growth of stress parallels the

growth of the linear function $U[\ ]$, and the difference between flow stress and $U[\ ]$ depends nonlinearly on the strain-rate.

Substitution of (16) into (5) and (6) results in the infinite-time limit for the response of Model IV

$$\left\{\sigma - \frac{E d_0 \zeta}{c_0 K[\dot{\epsilon}_{p1}]}\right\} = \frac{E}{c_0 K[\dot{\epsilon}_{p1}]} \tag{19}$$

while the plastic strain-rate in (19) has the value

$$\{\dot{\epsilon}_{p1}\} = \frac{c_0 \dot{\epsilon}}{c_0 + d_0}. \tag{20}$$

Constant stress-rate loading

We also examine the large-time behavior predicted by the theories in constant stress-rate loading (load-control). For Model II the differential constitutive equation is substituted into the integrand of the integral equation for overstress [44, 59], or $\tilde{\epsilon}_{p1}$ is required to vanish at infinite time (stress), and we obtain

$$\{\sigma - g\} = (E - E_t)\frac{\dot{\sigma}}{E_t} k[\{\sigma - g\}]. \tag{21}$$

The limit (10) also applies in constant stress-rate loading, and the combination of (9) and (10) is consistent with (21) and (10).

The limits (9), (10) and (21) establish correspondence between tests at constant strain-rates and at constant stress-rates. We consider loading at a strain-rate $\dot{\epsilon}_0$ and another separate loading at a constant stress-rate $\dot{\sigma}_0$, where $\dot{\sigma}_0$ is related to $\dot{\epsilon}_0$ by the slope-limit (10). Because the rates are related in this way, the overstress limits in (9) and (21) are identical and the large-time responses for these loadings coincide (Fig. 2).

The transition to steady-state behavior where the limits apply occurs more gradually in constant stress-rate loading than in constant strain-rate loading (Fig. 2). To understand the reason for this we use the definition of total strain, the chain rule, and the flow law to write the slope for Model II in loading at the constant strain-rate $\dot{\epsilon}_0$

$$\frac{d\sigma}{d\epsilon} = E - \frac{\sigma - g[\epsilon]}{k[\sigma - g[\epsilon]]\,\dot{\epsilon}_0}. \tag{22}$$

In constant stress-rate loading the strain-rate equals $(d\epsilon/d\sigma)\dot{\sigma}$, and loading at the stress-rate $\dot{\sigma}_0$ ($\dot{\sigma}_0 = E_t\dot{\epsilon}_0$) results in the stress–strain slope

$$\frac{d\sigma}{d\epsilon} = \frac{E}{1 + \dfrac{\sigma - g[\epsilon]}{k[\sigma - g[\epsilon]]E_t\dot{\epsilon}_0}}. \tag{23}$$

The difference between the constitutive equations for the slopes in (22) and (23) causes the difference between transient responses in stress- and strain-control. Similar differences occur between the slopes and transient responses of the other models in stress- and strain-control (Fig. 2).

For Models III and IV the limits (16)–(20) also apply in constant stress-rate loading. For both models the endochronic time has different values in the stress- and strain-controlled tests with respective rates $\dot{\sigma}_0$ and $\dot{\epsilon}_0$, and technically the limits (17, 19) both have different values in the stress- and strain-controlled tests. However this difference is negligible, and the steady-state responses approximately coincide in stress- and strain-control (Fig. 2).

The infinite-time limit for the slope of Model I in constant stress-rate loading is

$$\left\{\frac{d\sigma}{d\epsilon}\right\} = \frac{E\dot{\sigma}}{Ea_0 + \dot{\sigma}}. \tag{24}$$

Large values of a_0 are required to model the data used here, and the slope in (24) may be approximated as zero. The limit analogous to (13) but for Model I in stress-control could not be determined. In the tests with rates $\dot{\sigma}_0$ and $\dot{\epsilon}_0$ the responses do not merge (Fig. 2).

USE OF THE LIMITS TO FIT DATA

The infinite-time limits provide approximate relationships for the steady-state responses of the models at small stress and strain. From (9) and (10) we have the approximations

$$\frac{\sigma - g}{k[\sigma - g]} \approx (E - E_t)\dot{\epsilon} \tag{25}$$

and

$$\frac{d\sigma}{d\epsilon} \approx E_t. \tag{26}$$

Numerical solutions indicate that (25) and (26) apply at very small stress and strain (Fig. 3), and we use these to fit Model II to experimental data.

First experimental flow stress is plotted vs the log of the strain-rate at one fixed value of strain. The plot is extrapolated to low strain-rates until the stress-log of strain-rate curve turns flat. This stress level represents an estimate for $g[\ ]$ at the fixed strain of interest, and the process may be repeated to estimate $g[\ ]$ at other strains. Relaxation tests may also be used to estimate values of $g[\ ]$ at chosen strains [60]. The steady-state slope E_t in $g[\ ]$ is prescribed by using (26) under the approximation of linear experimental strain-hardening at sufficient strain.

With the representation of $g[\ ]$ chosen, constants in $k[\ ]$ are determined from (25) by substituting the stresses, strains, and strain-rates of the data points into (25). The number of data points fitted corresponds to the number of constants in the representation of $k[\ ]$, and because our interest is not quantitative reproduction of data, we use two constants.

For Model I the limit (13) corresponds to $W_{p1} = \infty$, and a very large strain (time) is necessary for the limit to apply; i.e. for stress to reach its constant bound and slope to vanish. However, (13) provides an approximate relationship for steady-state behavior at small stress, strain and plastic work

$$F[W_{p1}] \approx \sigma\,(\log_e[a_0/\dot{\epsilon}])^{1/b_0}. \tag{27}$$

Numerical solutions indicate the validity of (27) at infinitesimal strain. Both (13) and (27) indicate that a_0 must be chosen larger than the largest strain-rate of interest so that the log-function is positive. To fit data first a_0 and b_0 may be chosen. Then (27) may be used to determine $F[\ ]$ corresponding to experimental values of stress, strain, and plastic work. This requires estimates of W_{p1} for the data points of interest. However in this approach $F[\ ]$ is determined without any input of the experimental stress–strain slope which the model should predict at the data points. Different choices for a_0, b_0 result in widely different values of both $F[\ ]$ and the stress–strain slope.

To prescribe the slope we formally differentiate (27) or apply the approximation $\ddot{\epsilon}_{p1} \approx 0$ and obtain

$$\frac{dF[W_{p1}]}{dW_{p1}} \approx \frac{F[W_{p1}]\sigma'}{\sigma^2(1 - \sigma'/E)} \tag{28}$$

where $\sigma' = d\sigma/d\epsilon$. From (28) the stress–strain slope vanishes when $F[\ ]$ becomes constant at large plastic work, and this is consistent with (13).

To fit data we follow [45] and use

$$F[W_{p1}] = f_0 - f_1 \exp[-f_2 W_{p1}]. \tag{29}$$

Here f_2 is used as a dimensional constant specified in the Appendix. We first choose an

arbitrary large value or $F[\ ]$ at the first (static) data point to be fitted.† This value of $F[\ ]$ is substituted into (28) together with the experimental stress and stress–strain slope of the first data point. This specifies the slope at the first data point and determines f_1. Next f_0 is determined from (29) using the preselected value of $F[\ ]$ at this data point.

Next (29) is used to compute the value of $F[\ ]$ at thj second data point; and with $F[\ ]$ known at two data points, (27) is used to determine the constants a_0 and b_0. From (28) the representation of $F[\ ]$ in (29) allows specifications of the stress–strain slope at only one data point.

The predicted responses are nearly insensitive to the initial choice of $F[\ ]$ at the first data point. Different choices for the starting value of $F[\ ]$ result in different values for the material constants, but the stress–strain behavior is preserved. However different choices for the dimensional constant f_2 and the different representations of $F[\ ]$ significantly affect the curvatures of the responses [47].

For Models III and IV the limits (16) and (17), and (16) and (19) approximately apply at infinitesimal strain and represent the steady-state behavior of the responses (Figs. 5 and 6). To fit data an arbitrary value for d_0 is selected first. Then c_0 is determined by using (16) to prescribe the experimental slope at the first (static) data point under the approximation of linear steady-state strain-hardening. Different choices for d_0 are absorbed by correspondingly different values of c_0 and the constants in $K[\ ]$ while the stress–strain behavior remains unchanged.

Next K_2 in (7) is selected as a dimensional constant, and K_0, K_1 are determined by substituting the stresses, strains, and strain-rates of the two data points into the limits (17) or (19). Different values of K_0 are required to fit Models III and IV to the same data. If additional constants are added to the representation of $K[\ ]$ in order to fit more data points, the same procedure may be employed, and the limits provide a system of equations for the unknown constants.

For Model IV the plastic strain-rate in (5) is not constant until (16) applies, and the endochronic time in (19) is not equal to $K[\dot{\epsilon}_{p1}]\epsilon_{p1}$. However, only the stress, strain, and strain-rate are known in experiments; and the endochronic time must be estimated in order to use (19). To facilitate fitting data we use the approximation

$$\zeta \approx K[\dot{\epsilon}_{p1}]\epsilon_{p1} \tag{30}$$

and this results in an accurate fit of the experimental data points. The relative difference between numerical solutions of Model IV and the limit (19) using (30) is approx. $10^{-3}\%$ at infinitesimal strain and at all the strain-rates, and this indicates that (30) is acceptable in (19).

Table 1 lists additional responses of Models I–IV at strain-rates corresponding to experimental data points not used in fitting the models. Although only two data points were fitted, the particular functions used in the constitutive equations provide reasonable fits of additional steady-state data points and reasonable representations of the experimental rate-dependence.

BEHAVIOR PREDICTED UNDER JUMPS IN STRAIN-RATE OR STRESS-RATE

We examine the behavior predicted by each theory under instantaneous jump increases (decreases) in the strain- or stress-rates. The constant strain-rates before and after the jump are respectively denoted by $\dot{\epsilon}^-$ and $\dot{\epsilon}^+$, where $\dot{\epsilon}^+ = \delta\dot{\epsilon}^-$. A strain-rate increase corresponds to $\delta > 1$ and a strain-rate decrease with increasing strain corresponds to $0 < \delta < 1$; strain-rate reversal and unloading correspond to $\delta < 0$.

From the definition of total strain and the chain rule the slope for each model before the strain-rate jump is

$$\frac{d\sigma^-}{d\epsilon} = E - E\frac{\dot{\epsilon}^-_{p1}}{\dot{\epsilon}^-}. \tag{31}$$

†$F[\ ]$ is taken large in comparison with the stresses of data points being fitted.

The superscripts − and + respectively denote values before and after the jump. After the strain-rate jump the slope for each model is

$$\frac{d\sigma^+}{d\epsilon} = E - E\frac{\dot{\epsilon}_{p1}^+}{\dot{\epsilon}^+}. \tag{32}$$

Combining (31) and (32) *at* the instant of the strain-rate jump gives

$$\frac{d\sigma^+}{d\epsilon} = E - \left(\frac{\dot{\epsilon}^-}{\dot{\epsilon}^+}\right)\left(\frac{\dot{\epsilon}_{p1}^+}{\dot{\epsilon}_{p1}^-}\right)\left(E - \frac{d\sigma^-}{d\epsilon}\right). \tag{33}$$

At the point where the strain-rate change occurs the plastic strain-rates of Models I, II, IV are respectively the same both before and after the strain-rate jump; i.e. $\dot{\epsilon}_{p1}^+ = \dot{\epsilon}_{p1}^-$. Using this relationship (33) becomes

$$\frac{d\sigma^+}{d\epsilon} = E - \frac{1}{\delta}\left(E - \frac{d\sigma^-}{d\epsilon}\right). \tag{34}$$

For Model III the plastic strain-rate changes with the jump, and (33) with (3) and (4) becomes

$$\frac{d\sigma^+}{d\epsilon} = E - \frac{K[\delta\dot{\epsilon}^-]}{K[\dot{\epsilon}^-]}\left(E - \frac{d\sigma^-}{d\epsilon}\right)\text{sign}[\delta]. \tag{35}$$

To examine the predictions of the models under jumps in the stress-rate we let $\dot{\sigma}^+ = \gamma\dot{\sigma}^-$, and a stress-rate increase corresponds to $\gamma > 1$. A stress-rate decrease with continued loading corresponds to $0 < \gamma < 1$, and a stress-rate reversal (unloading) corresponds to $\gamma < 0$. From the definition of total strain

$$\frac{d\epsilon}{d\sigma} = \frac{1}{E} + \frac{\dot{\epsilon}_{p1}}{\dot{\sigma}}. \tag{36}$$

Using (36) both before and after the stress-rate jump results in a relationship between the stress–strain slopes before and after the jump. For Models I, II and IV *at* the point of the jump

$$\frac{d\sigma^+}{d\epsilon} = E\left[1 + \frac{1}{\gamma}\left(E\Big/\frac{d\sigma^-}{d\epsilon} - 1\right)\right]^{-1}. \tag{37}$$

We cannot obtain a similar relationship for Model III, but a transcendental equation for the slope $d\sigma/d\epsilon^+$ can be solved numerically.

We examine the rate changes in regions where the steady-state conditions approximately apply; where $d\sigma/d\epsilon^- \ll E$. The slopes of Models I, II and IV before and after jumps in the strain- (stress-) rate are related only by the ratio δ (γ). However the slopes of Model III are related both by the ratio δ (γ) and the value of the strain- (stress-) rate preceding the jump, and this causes significantly different responses for Model III. For a large strain-rate increase (decrease) the terms with $1/\delta$ are negligible (dominant) in (34), and for a large stress-rate increase (decrease) the terms with $1/\gamma$ are negligible (dominant) in (37). For Model III the terms with δ and γ are neither dominant nor negligible. The effects of large rate increases and decreases are summarized in Table 2 and demonstrated in Figs. 3–10 for Models I–IV.

We compare the response following the strain-rate change with the response which occurs

Table 2. Stress–strain slopes immediately following large strain- (stress-) rate increases and decreases

Approximate $\frac{d\sigma^+}{d\epsilon}$ for:	Large δ $\delta \gg 1$	Small δ $0<\delta\ll 1$	Large γ $\gamma \gg 1$	Small γ $0<\gamma\ll 1$
Models I, II, IV	E	$-\frac{E}{\delta}$	E	$\gamma\frac{d\sigma^-}{d\epsilon}$
Model III	Positive $<E$	Negative $>-\frac{E}{\delta}$	Positive $<E$	Small Positive

through initial loading at the strain-rate $\dot{\epsilon}^+$. For reference the response to initial loading at the rate $\dot{\epsilon}^+$ is called the "pure response," and the response to loading with the combined rates $\dot{\epsilon}^-$, $\dot{\epsilon}^+$ is called the "jump response."

For Model II the approximation (25) applies for the steady-state behavior of the pure and jump responses, and in both cases the strain-rate in (25) is $\dot{\epsilon}^+$. Consequently the pure and jump responses merge when the jump response returns to steady-state behavior, and the return to steady-state is very rapid (Fig. 3). The jump responses to strain-rate increases and decreases rapidly merge with the corresponding pure responses before significant strain accumulates, and Model II predicts no significant memory for the prior strain-rate values; it models no strain-rate history effect (SRHE).†

For Model I the steady-state approximation (27) contains the strain-rate $\dot{\epsilon}^+$ for both the jump and pure responses, and the jump response rapidly returns to steady-state behavior (Fig. 4). However, the plastic work in (27) is different for the two responses, and this causes different stresses in (27) for the jump and pure responses. The responses remain apart after the jump response has returned to steady-state behavior, and Model I predicts an SRHE (Fig. 4). The relative difference between plastic work of the two responses decreases with increasing strain, and from (27) the responses eventually merge. For the data used here the responses merge very slowly (Fig. 4).

For Models III and IV the endochronic times in (17) and (19) both have different values for the jump and pure responses. This causes different steady-state flow stresses for the jump and pure responses, and Models III and IV demonstrate SRHE's (Figs. 5 and 6). For each model the difference between endochronic times of the jump and pure responses, relative to the present values of ζ, decreases with increasing strain; the responses eventually merge. For the data and strain-rates used here the SRHE's last over very large strain.

DISCUSSION

At the strain-rate $10^{-5}\,s^{-1}$ the responses of Models I, II and IV are very similar, but at higher strain-rates the responses of Model I differ distinctly from the responses of Models II and IV (Figs. 1, 3–5). Models II and IV predict rate-independent steady-state slopes, and fitting the

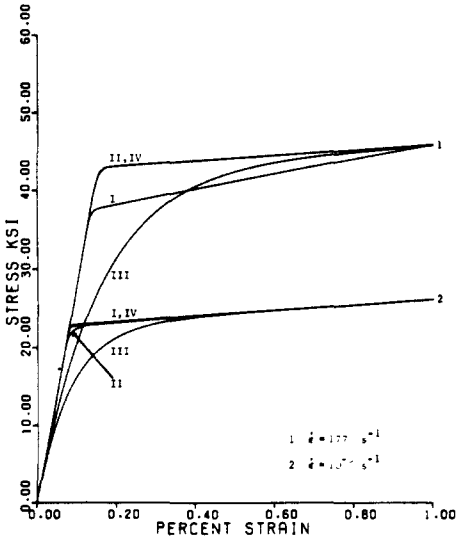

Fig. 1.

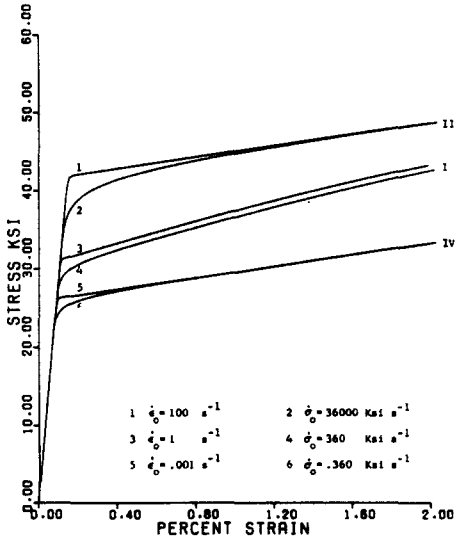

Fig. 2.

Fig. 1. Stress–strain responses for Models I–IV at the two strain-rates used to fit data. Models II–IV predict the same constant, rate-independent steady-state slopes while Model I predicts nonconstant and rate-dependent slopes.

Fig. 2. Responses of Models I, II and IV at various constant stress- (strain-) rates. Different rates are used for each model to provide spacing between the responses, and the applied stress-rate is always 360 Ksi times the applied strain-rate. For each model the transition to steady-state is more gradual in stress-control, and the responses of Model II (Model IV) coincide in stress- and strain-control.

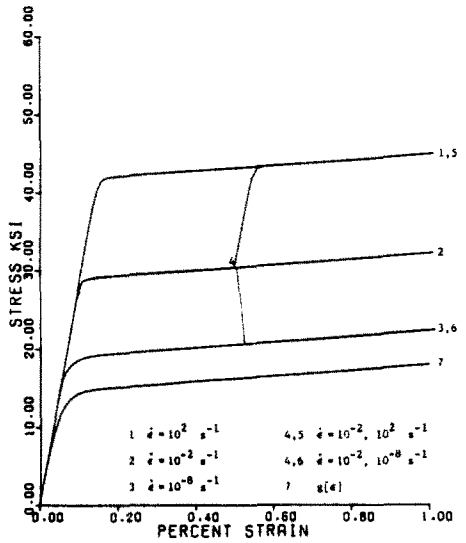

Fig. 3.

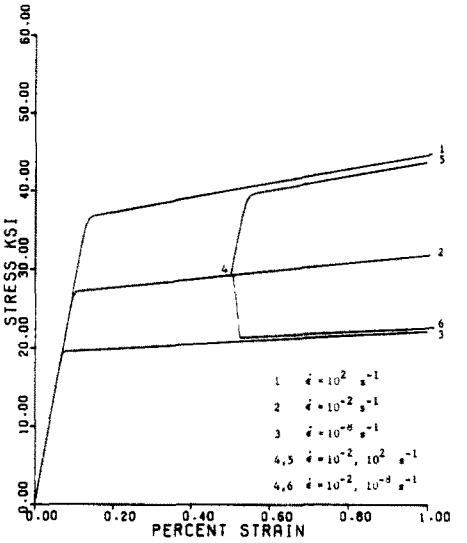

Fig. 4.

Fig. 3. Stress–strain responses of Model II at various constant strain-rates and following strain-rate jumps. The large strain-rate increase produces elastic slope while the strain-rate decrease produces negative slope and decreases in stress. The equilibrium responses $g[\ ]$ is also shown.

Fig. 4. Responses of Model I for the same piecewise constant strain-rates of Fig. 3. The plastic work in the flow law produces a strain-rate history effect, and the responses merge after very large strain.

models to the same experimental slope at $10^{-5}\,s^{-1}$ causes identical steady-state slopes for these models at all strain-rates. This permits their steady-state responses to approximately coincide at all strain-rates (Figs. 1, 3 and 5). For Model I the plastic work in (28) is different for different stress–strain responses, and this causes the steady-state slopes for Model I to be rate-dependent. At higher strain-rates the steady-state slope for Model I is significantly greater than the slopes for Models II and IV, and this causes the differences between the steady-state responses of Model I and Models II, IV. This difference between responses also occurs at strain-rates below $10^{-5}\,s^{-1}$, although the difference is harder to see for the scale of Figs. 3–5.

The responses of Models I, II, and IV rapidly attain steady-state at small strain, while the responses of Model III require much larger strain before reaching steady-state (Fig. 1). Different functions may be used in the constitutive equations to modify the sharp (gradual) transitions to

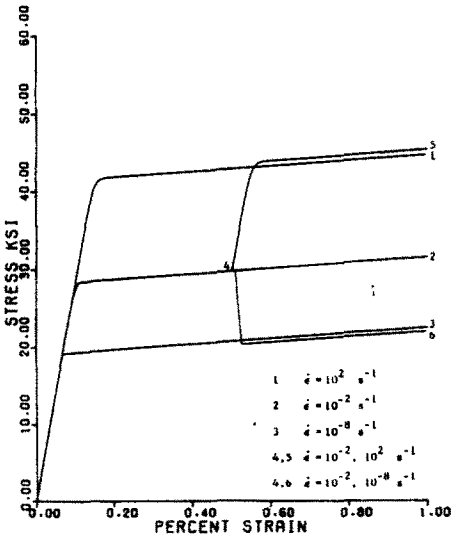

Fig. 5. Responses of Model IV for the same piecewise constant strain-rates of Figs. 3 and 4. The endochronic time models a strain-rate history effect opposite that of Model I in Fig. 4. Responses from the origin appear elastic despite lack of a yield surface.

steady-state behavior. For Models I and II the functions $F[\ ]$ and $g[\ ]$ respectively may be changed to modify transient stress–strain responses while the flow laws remain unchanged [47, 57].† Alternatively for Models III and IV the flow laws must be changed to change the transient responses [39]. Here we compare qualitative predictions of the models and do not attempt to fit transient experimental behavior.

The use of the steady-state approximations to fit the models to data requires that the data points correspond to regions of steady-state solutions to the constitutive equations. In Table 1 the difference between the experimental data point and the numerical response of Model III at the strain-rate 177 s^{-1} occurs because the computed response has not yet reached steady-state at the strain of this data point.

From (13) the constant strain-rate responses of Model I are bounded while the responses of the other models are unbounded.‡ The stress of Model I may reach its bound either at infinitesimal strain or at extremely large strain depending on the data fitted and the representation of $F[\ ]$. In (8) the endochronic time is unbounded in strain, but in (1) $F[\ ]$ is bounded in the plastic work, and the fact that $F[\ ]$ is bounded causes the bounded responses of Model I. This suggests a possible increase in the flexibility of Model I by using an unbounded F-function to obtain unbounded responses similar to the predictions of other models. The dependence of $F[\ ]$ upon plastic work and the impact of $F[\ ]$ upon stress–strain behavior through (27) and (28) make determination of a suitable unbounded function difficult, and none has been obtained thus far.

When (9) approximately applies the response from Model II parallels the equilibrium response $g[\ ]$ for any strain-rate (Fig. 3). Similarly the steady-state response of Model III parallels the curve represented by $U[\zeta, \dot{\epsilon}]$ in (17) and (18), and the response of Model IV in (19) parallels the curve represented by $(c_0 + d_0)U[\zeta, \dot{\epsilon}_{p1}]/c_0$. However $U[\ ]$ does not represent an equilibrium stress–strain curve. While $g[\ ]$ is rate-independent and a lower bound for the stress–strain behavior in monotonic loading, $U[\ ]$ is rate-dependent and decreases with decreasing strain-rates.

For each of the models in Fig. 2 the rates in the stress- and strain-controlled tests are related by the constant ratio $\dot{\sigma}_0/\dot{\epsilon}_0$. This ratio corresponds to the constant steady-state slopes in (10) and (16) but not the nonconstant slope in (28). While the steady-state responses of Models II and IV in stress- and strain-control respectively merge, the responses of Model I do not merge (Fig. 2). These tests also may be performed with Model III, and the responses merge. The predictions may be compared with similar experiments in order to favor selection of a particular theory.

Each model predicts sharper responses in constant strain-rate loading than in constant stress-rate loading because of the different stress–strain nonlinearity of the constitutive equations; e.g. eqns (22) and (23) and Fig. 2. The steady-state limits are attained more slowly in stress-control than in strain-control, and this represents a bias between the responses which each model predicts in stress- and strain-control. The difference between transient responses in stress- and strain-control increases with increasing stress- (strain-) rates (Fig. 2).

Models I, II and IV predict approximately elastic slopes for the responses immediately following large strain-rate increases; Table 2 and Figs. 3–5. Additional models not examined here will also predict elastic slopes providing their plastic strain-rates do not jump with an instantaneous change in the total strain-rate. However, Model III predicts less than elastic slope following the same large strain-rate increases (Fig. 6). This prediction differs from the elastic slopes reported in experiments [1–3, 6–8, 10, 12] and supports selection of Models I, II and IV over Model II.

For Models I, II and IV a large strain-rate decrease (e.g. $\delta = 10^{-2}, 10^{-4}$) immediately causes large negative stress–strain slope; Table 2, Figs. 3–5. The stress decreases as strain increases. With further straining the slopes become positive again, and stress and strain both increase again. Model III also predicts negative slopes immediately following large strain-rate decreases, but the magnitude of the slope is significantly less than that of the other models (Fig. 6).

†Some choices for constants in $F[\ ]$ and for representations of $F[\ ]$ cause stress–strain responses with temporarily increasing slopes; with upward curvatures.

‡The finite-deformation representation of Model I [45] requires separate examination of the infinite-time limits and steady-state approximations.

All four models predict *biases* between responses following sudden changes in the stress- and strain-rates (Figs. 3–10). A large stress-rate increase produces elastic slope in the responses of Models I, II and IV. However, γ must be orders of magnitude greater than δ to obtain the same approximation of elastic slope. Model III predicts inelastic slope following large stress-rate increases, and again $\gamma \gg \delta$ in order to obtain the same slopes after stress- and strain-rate increases. As part of this bias the jump responses return to steady-state behavior more quickly after strain-rate increases.

All of the models show a strong bias between the responses to sudden stress- and strain-rate decreases. Large stress-rate decreases produce *positive* stress–strain slopes while large strain-rate decreases produce *negative* slopes (Figs. 3–10). The servocontrolled experiments in [2] support these different predictions. Because of the small slope following a stress-rate decrease, small increases in stress produce very large increases in strain.

Model II demonstrates *stress-rate history effects* although it does not predict strain-rate history effects, and this is part of its bias between responses in stress- and strain-control (Fig. 7). The stress-rate history effect occurs after a stress-rate increase because the soft response in stress-control returns to steady-state behavior slowly over significant strain. Because of its small slope, the response to a stress-rate decrease also requires significant strain to return to steady-state behavior, and this causes a longer stress-rate history effect. In (21) the limiting overstress is identical for the response to a stress-rate increase (decrease) and the corresponding pure response, and the stress-rate history effect fades away when the responses return to steady-state and merge.

Models I, III and IV also predict stress-rate history effects because of the soft responses to stress-rate increases and the small slopes corresponding to stress-rate decreases (Figs. 8–10). The plastic work and endochronic time have different values for the responses to stress-rate increases (decreases) and the pure responses, and this causes stress-rate history effects which remain after the responses return to steady-state; which last over large strain.

The biases between responses in stress- and strain-control indicate need for caution in performing and interpreting experiments which are linked with these theories. It is important to reliably categorize experiments as stress-controlled, strain-controlled, or neither, in order to compare the experiments and theories. Additional biases corresponding to stress- and strain-rate reversals are detailed in [58].

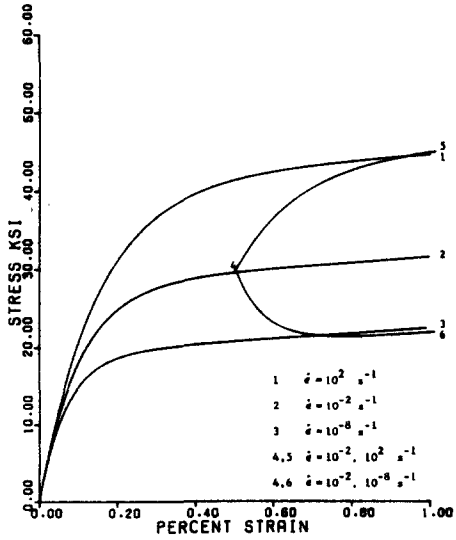

Fig. 6.

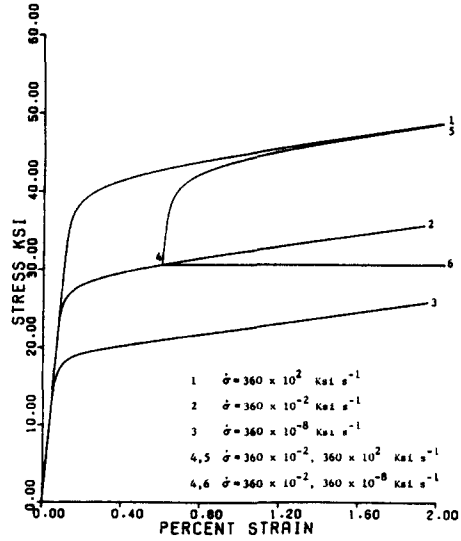

Fig. 7.

Fig. 6. Responses of Model III for the piecewise constant strain-rates of Figs. 3–5. The strain-rate increase produces inelastic slope.

Fig. 7. Responses of Model II at constant stress-rates and following stress-rate jumps. The large stress-rate increase produces elastic slope, and the stress-rate decrease produces extremely small, positive slope.

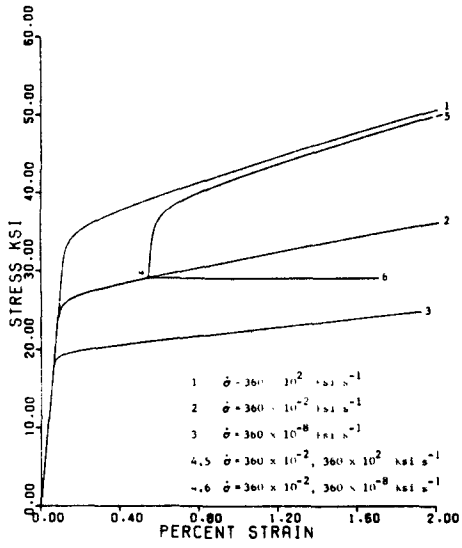

Fig. 8.

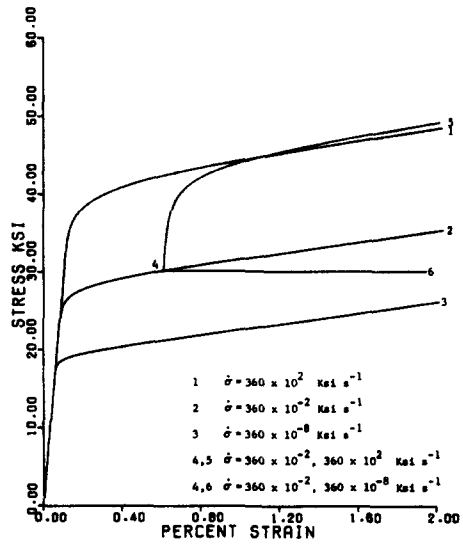

Fig. 9.

Fig. 8. Responses of Model I for piecewise constant stress-rates, indicating the bias between stress- and strain-control.

Fig. 9. Stress–strain responses of Model IV for the piecewise constant stress-rates of Figs. 7 and 8. The stress-rate history effect parallels the model's strain-rate history effect and the jump and pure responses cross.

Models I, III and IV predict SRHE's because their flow laws contain continuous measures of past plastic deformation through W_{pl} and ζ. Large strain-rate changes produce large differences between the plastic work and endochronic time of the jump and pure responses, causing large strain-rate history effects and large strain-intervals before responses merge. Model II predicts no SRHE because the jump response rapidly returns to steady-state behavior and because the model has no continuous memory for prior deformation during monotonic loading.†

The difference in the definitions of W_{pl} and ζ results in opposite manifestations of the SRHE for Model I and Models III, IV (Figs. 4–6). The response of Model I to a strain-rate

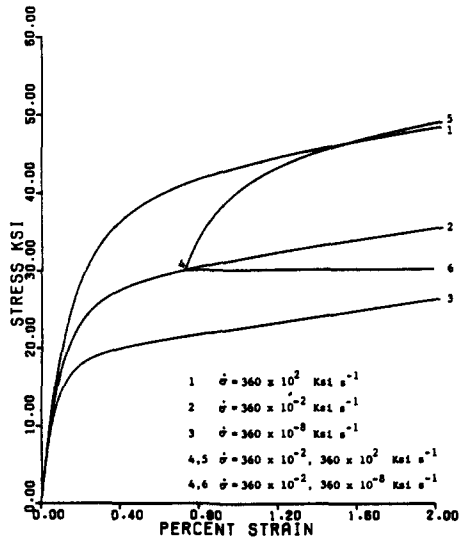

Fig. 10. Responses of Model III for piecewise constant stress-rates. The stress-rate increase produces inelastic slope.

†Model II has discontinuous memory for prior plastic deformation during cycling[58, 59].

increase remains below the corresponding pure response curve while the jump response of Model IV following a strain-rate increase crosses above the pure response. The jump response of Model III also crosses above the pure response, but more gradually and after a larger interval of strain.

Because the plastic work in Model I is greater for the pure response than for the jump response, $F[\ ]$ is greater for the pure response, and the responses of Model I cannot cross. In Models III and IV the endochronic time is smaller for the pure response than for the jump response, and this distinction permits the responses to cross. The difference between W_{p1} and ζ also causes the different strain- (stress-) rate history effects of Model I and Models III, IV corresponding to strain- (stress-) rate decreases.

The different SRHE's indicate ways in which the constitutive equations of all the theories may be modified to represent different manifestations of memory for prior plastic deformation. Experiments with different metals [1–3, 6–8, 10, 12, 16, 22] support the different predictions of Models I, II, and IV.

Models I–IV do not use yield surfaces, and the flow laws apply at all times. At the start of loading from the origin the plastic strain-rates are zero, and their growth is gradual. The initial responses are approximately linear, and the regions of linear behavior increase with increasing strain-rates. At low stresses the initial linear responses approximate elastic behavior, but at higher stresses the linear responses are significantly inelastic. This distinction is highlighted by the creep and relaxation behavior predicted at stress–strain points within these linear regions.

At low stress, such as 5 Ksi, Models I, II and IV predict no creep or relaxation for time up to 10^3 yr. At larger stresses these models predict significant creep and relaxation after preloading within the regions of initial linear stress–strain behavior (Table 3). After preloading to 28 Ksi the creep responses of Models II and IV remain very close for large times up to 10^3 yr, but at higher stresses such as 56 Ksi the difference in these responses increases rapidly for a time scale in years (Table 3). For Model I the creep response at 28 Ksi parallels the responses of Models II and IV for times up to years, but at large stress (56 Ksi) the creep response of Model I is extremely large. The large creep response makes Model I impractical for the representation of creep behavior for the data fitted here.

For Model II the creep response is bounded by the equilibrium response $g[\ ]$, and creep terminates when the total strain equals $g^{-1}[\sigma]$[43]. For Model IV the creep-rate continually decreases as strain increases, and for Model I the creep-rate reaches a constant, steady-state value after the plastic work increases and $F[\ ]$ becomes constant.

After preloading in a region of linear stress–strain behavior, or after preloading to regions of steady-state behavior, the relaxation responses of Models I, II and IV agree closely over large times exceeding 10^3 yr (Table 3). At extremely large time the equilibrium response $g[\ ]$ provides

Table 3. Creep and relaxation responses of Models I, II and IV

Initial Stress Initial Strain	28 Ksi .1 %			56 Ksi .2 %		
Time	10^2 s	10^1 yr	10^3 yr	10^2 s	10^1 yr	10^3 yr
Creep Strain Model I %	1.17	4.57	9.82	10^4	10^9	10^{13}
Creep Strain Model II %	1.24	3.03	3.43	8.92	10.7	11.1
Creep Strain Model IV %	1.36	3.79	4.84	13.0	18.0	20.1
Relaxation Stress Model I Ksi	20.9	16.3	14.6	21.5	16.8	15.1
Relaxation Stress Model II Ksi	20.1	15.6	14.7	20.9	16.4	15.5
Relaxation Stress Model IV Ksi	20.7	15.6	13.8	20.9	15.7	13.9

The creep and relaxation responses correspond to preloading in the region of initial linear behavior. The creep responses of Model III match the creep responses of Model IV.

a lower bound for the relaxation stress of Model II while the stresses of Models I and IV continue to relax to zero. However, this distinction is not significant for times shorter than centuries.

Model III does not predict any relaxation behavior. However, it predicts creep behavior nearly identical to the creep responses of Model IV. A negligible difference between responses occurs because of different values of K_0 in the K-functions of these models.

Models I, II and IV predict relaxation from 28 Ksi which is much faster than the experimental relaxation in [1], and at 30 s the predicted stress-decrease is approximately four times the experimental value. The models need increased flexibility in order to represent both the relaxation and stress–strain behavior of this material. They need additional, separate repositories for modeling relaxation (creep) behavior and modelling stress–strain behavior so that experimental relaxation- (creep-) rates can be matched after the steady-state stress–strain behavior has been prescribed.

Because Model II has no memory for the prior strain-rate history, it predicts identical relaxation (creep) responses after preloading to the same point with different strain-rate combinations. Alternatively the plastic work and endochronic time in Models I and IV have different values for different strain-rate histories, and the relaxation (creep) responses of these models are slightly different when different strain-rate histories are used to preload to the same stress–strain point.

Similarly relaxation causes small changes in the plastic work and endochronic time of Models I and IV. Reloading after relaxation produces a steady-state stress–strain response which differs slightly from the original pure response free of relaxation. For Model II the response to reloading after relaxation coincides with the original, pure response.

Acknowledgement—Contributions from Dr. Erhard Krempl are gratefully acknowledged. This work was supported by the National Science Foundation.

REFERENCES

1. E. Krempl, An experimental study of room-temperature rate sensitivity, creep, and relaxation of aisi type 304 stainless steel. *J. Mech. Phys. Solids* **27**, 363–375 (1979).
2. D. Kujawski, V. Kallianpur and E. Krempl, An experimental study of uniaxial creep, cyclic creep, and relaxation of aisi type 304 stainless steel at room temperature. *J. Mech. Phys. Solids* **28**, 129–148 (1980).
3. D. Kujawski and E. Krempl, The rate- (time-) dependent behavior of the Ti-7Al-2Cb-1Ta titanium alloy at room temperature under monotonic and cyclic loading. *Trans. ASME, J. Appl. Mech.* **48**, 55–63 (1981).
4. C. Albertini and M. Montagnani, Dynamic uniaxial and biaxial stress–strain relationships for austenitic stainless steels. *Nucl. Engng Design* **57**, 107–123 (1980).
5. C. Albertini and M. Montagnani, Wave propagation effects in dynamic loading. *Nucl. Engng Design* **37**, 115–124 (1976).
6. P. E. Senseny, J. Duffy and R. H. Hawley, Experiments on strain-rate history and temperature effects during the plastic deformation of close-packed metals. *Trans. ASME, J. Appl. Mech.* **45**, 60–66 (1978).
7. A. M. Eleiche and J. D. Campbell, Strain-rate effects during reverse torsional shear. *Exp. Mech.* **16**, 281–290 (1976).
8. J. D. Campbell and T. L. Briggs, Strain-rate history effects in polycrystalline molybdenum and niobium. *J. Less Common Metals* **40**, 235–250 (1975).
9. B. Dodd, R. C. Stone and J. D. Campbell, The strain-rate sensitivity of 304L austenitic stainless steel in uniaxial tension. Oxford University Rep. 1069/73 (1973).
10. R. A. Frantz, Jr. and J. Duffy, The dynamic stress–strain behavior in torsion of 1100-0 aluminum subjected to a sharp increase in strain rate. *Trans. ASME, J. Appl. Mech.* **39**, 939–945 (1972).
11. J. E. Lawson and T. Nicholas, The dynamic mechanical behavior of titanium in shear. *J. Mech. Phys. Solids* **20**, 65–76 (1972).
12. T. Nicholas, Strain rate and strain-rate history effects in several metals in torsion. *Exp. Mech.* **11**, 370–374 (1971).
13. S. K. Samanta, Dynamic deformation of aluminum and copper at elevated temperatures. *J. Mech. Phys. Solids* **19**, 117–135 (1971).
14. J. Klepaczko, Effects of strain-rate history on the strain hardening curve of aluminum. *Arch. Mech. Sto.* **19**, 211–228 (1967).
15. C. J. Maiden and S. J. Green, Compressive strain-rate tests on six selected materials at strain rates from 10^{-3} to 10^4 sec^{-1}. *Trans. ASME, J. Appl. Mech.* **33**, 496–504 (1966).
16. R. N. Orava, G. Stone and H. Conrad, The effects of temperature and strain rate on the yield and flow stresses of alpha-titanium. *Trans. ASME* **59**, 171–184 (1966).
17. C. H. Karnes and E. A. Ripperger, Strain rate effects in cold worked high-purity aluminum. *J. Mech. Phys. Solids* **14**, 75–88 (1966).
18. K. Hoge, Influence of strain rate on mechanical properties of 6061-T6 aluminum under uniaxial and biaxial states of stress. *Exp. Mech.* **6**, 204–211 (1966).
19. U. S. Lindholm and L. M. Yeakley, Dynamic deformation of single and polycrystalline aluminum. *J. Mech. Phys. Solids* **13**, 41–52 (1965).
20. U. S. Lindholm, Some experiments with the split Hopkinson pressure bar. *J. Mech. Phys. Solids* **12**, 317–335 (1964).

21. F. E. Hauser, J. A. Simmons and J. E. Dorn, Strain rate effects in plastic wave propagation. In *Response of Metals to High Velocity Deformation* (Edited by P. G. Shewmon and V. F. Zackay), pp. 93–114. Interscience, New York (1961).
22. Z. S. Basinski and J. W. Christian, The influence of temperature and strain rate on the flow stress of annealed and decarburized iron at subatomic temperatures. *Australian. J. Phys.* **13**, 299–308 (1960).
23. C. J. Maiden and J. D. Campbell, The static and dynamic strength of a carbon steel at low temperatures. *Phil. Mag.* **3**, 872–885 (1958).
24. C. E. Pugh and D. N. Robinson, Some trends in constitutive equation model development for high-temperature behavior of fast-reactor structural alloys. *Nucl. Engng Design* **48**, 269–276 (1978).
25. J. R. Ellis, D. N. Robinson and C. E. Pugh, Behavior of annealed type 316 stainless steel under monotonic and cyclic biaxial loading at room temperature. *Nucl. Engng Design* **47**, 115–123 (1978).
26. J. F. Thomas, Jr. and F. L. Yaggee, Stress relaxation in solution-annealed and 20 per cent gold-worked type 316 stainless steel. *Met. Trans.* **6A**, 1835–1837 (1975).
27. H. Yamada and Che-Yu Li, Stress relaxation and mechanical equation of state in austenitic strainless steels. *Met. Trans.* **4**, 2133–2136 (1973).
28. J. J. Blass and W. N. Findley, Short-time, biaxial creep of an aluminum alloy with abrupt changes of temperature and state of stress. *Trans. ASME, J. Appl. Mech.* **38**, 489–501 (1971).
29. G. M. Brown, Inelastic deformation of an aluminum alloy under combined stress at elevated temperature. *J. Mech. Phys. Solids* **18**, 383–396 (1970).
30. T. T. Wang and E. T. Onat, Non-linear mechanical behavior of 1100 aluminum at 300°F. *Acta Mechanica* **5**, 54–70 (1968).
31. E. J. Sternglass and D. A. Stuart, An experimental study of the propagation of transient longitudinal deformations in elastoplastic media. *Trans. ASME, J. Appl. Mech.* **20**, 427–434 (1953).
32. B. E. K. Alter and C. W. Curtis, Effect of strain rate on the propagation of a plastic strain pulse along a lead bar. *J. Appl. Phys.* **27**, 1079–1085 (1956).
33. J. F. Bell and A. Stein, The incremental loading wave in the pre-stressed plastic field. *J. Mecanique* **1**, 395–412 (1962).
34. E. Convery and H. L. D. Pugh, Velocity of torsional waves in metals stressed statically into the plastic range. *J. Mech. Engng Sci.* **10**, 153–164 (1968).
35. C. H. Yew and H. A. Richardson, Jr., The strain-rate effect and the incremental plastic wave in copper. *Exp. Mech.* **9**, 366–373 (1969).
36. J. D. Campbell and A. R. Dowling, The behaviour of materials subjected to dynamic incremental shear loading. *J. Mech. Phys. Solids* 43–63 (1970).
37. Y. R. Rashid and M. N. Sharabi, Strain-rate dependent plasticity in thermo-mechanical transient analysis. *Nucl. Engng Design* **57**, 41–48 (1980).
38. H. C. Lin and H. C. Wu, Strain-rate effect in the endochronic theory of viscoplasticity. *Trans. ASME, J. Appl. Mech.* **43**, 92–96 (1976).
39. H. C. Wu and M. C. Yip, Strain rate and strain rate history effects on the dynamic behavior of metallic materials. *Int. J. Solids Structures* **16**, 515–536 (1980).
40. E. A. Ripperger and H. Watson, Jr., The relationship between the constitutive equation and one-dimensional wave propagation. In *Mechanical Behavior of Materials Under Dynamic Loads* (Edited by U. S. Lindholm), pp. 294–313. Springer-Verlag, New York (1968).
41. J. Lubliner, A generalized theory of strain-rate-dependent plastic wave propagation in bars. *J. Mech. Phys. Solids* **12**, 59–66 (1964).
42. N. Cristescu, Rate-type constitutive equations in dynamic plasticity. In *Problems in Plasticity* (Edited by A. Sawczuk), pp. 287–310. Nordhoff, Leyden (1974).
43. E. P. Cernocky and E. Krempl, A nonlinear uniaxial integral constitutive equation incorporating rate effects, creep, and relaxation. *Int. J. Non-Linear Mech.* **14**, 183–203 (1979).
44. E. P. Cernocky and E. Krempl, A theory of viscoplasticity based on infinitesimal total strain. *Acta Mech.* **36**, 263–289 (1980).
45. S. R. Bodner and Y. Partom, Constitutive equations for elastic-viscoplastic strain-hardening materials. *Trans. ASME, J. Appl. Mech.* **42**, 385–389 (1975).
46. S. R. Bodner and Y. Partom, Constitutive equations for cyclic loading of rate dependent materials. MML Report 51, Technion (1976).
47. S. R. Bodner and A. Merzer, Viscoplastic constitutive equations for copper with strain rate history and temperature effects. *Trans. ASME, J. Engng Mat. Tech.* **100**, 388–394 (1978).
48. E. W. Hart. Constitutive relations for the nonelastic deformation of metals. *Trans. ASME, J. Engng Mat. Tech.* **98**, 193–201 (1976).
49. R. W. Rhode and J. C. Swearengen, Deformation modeling applied to stress relaxation of four solder alloys. *Trans. ASME, J. Engng Mat. Tech.* **102**, 207–214 (1980).
50. A. Miller, An inelastic constitutive model for monotonic, cyclic and creep deformation, Parts I and II. *Trans. ASME, J. Engng Mat. Tech.* **98**, 97–113 (1976).
51. P. P. Gillis, Linearly viscoplastic material. *J. Appl. Phys.* **48**, 2845–2849 (1977).
52. J. H. Gittus, Development of constitutive relation for plastic deformation from a dislocation model. *Trans. ASME, J. Engng Mat. Tech.* **98**, 52–59 (1976).
53. A. R. S. Ponter and F. A. Leckie, Constitutive relationships for the time-dependent deformation of metals. *Trans. ASME, J. Engng Mat. Tech.* **98**, 47–51 (1976).
54. V. V. Sokolovsky, The propagation of elastic-viscous-plastic waves in bars. *Prik. Matematika i Mekhanika* **12**, 261–280 (1948).
55. L. E. Malvern, The propagation of longitudinal waves of plastic deformation in a bar of material exhibiting a strain-rate effect. *Trans. ASME, J. Appl. Mech.* **18**, 203–208 (1951).
56. P. M. Naghdi and S. A. Murch, On the mechanical behavior of viscoelastic/plastic solids. *Trans. ASME, J. Appl. Mech.* **30**, 321–328 (1963).
57. E. P. Cernocky and E. Krempl, Construction of nonlinear monotonic functions with selectable intervals of almost constant or linear behavior. *Trans. ASME, J. Appl. Mech.* **45**, 780–784 (1978).

58. E. P. Cernocky, Comparison of the unloading and reversed loading behavior of three viscoplastic constitutive theories. *Int. J. Non-Linear Mech.*, forthcoming.
59. E. P. Cernocky and E. Krempl, A theory of thermoviscoplasticity based on infinitesimal total strain. *Int. J. Solids Structures* **16**, 723–741 (1980).
60. M. C. M. Liu and E. Krempl, A uniaxial viscoplastic model based on total strain and overstress. *J. Mech. Phys. Solids* **27**, 377–391 (1979).
61. K. C. Valanis, A theory of viscoplasticity without a yield surface—I. *Arch. Mech. Sto.* **23**, 517–533 (1971).

APPENDIX

Materials functions and properties used in the numerical experiments

(1) $E = 28{,}000$ Ksi $\quad \frac{d\sigma}{d\epsilon} = 360$ Ksi at $\epsilon = 0.01$, $\dot{\epsilon} = 10^{-5}\,s^{-1}$.

(2) Parameters corresponding to Model I and $F[\ ]$ in eqn (29).

$b_0 = 1.02367$ $\quad a_0 = 1.1158 \times 10^{13}\,s^{-1}$

$f_0 = 1531.04$ Ksi $\quad f_1 = 663.67$ Ksi $\quad f_2 = 1$ Ksi^{-1}.

(3) Parameters and functions corresponding to Model II.
The $g[\ ]$-function is selected from [57]:

$$g[\epsilon] = E_t\epsilon + \frac{(E - E_t)}{2R\tanh[RX_f - 3]} \log_e\left[\frac{\cosh[U]}{\cosh[V]}\right]$$

where $U = R(X_f + \epsilon) - 3$, $V = R(X_f - \epsilon) - 3$, $E_t = 360$ Ksi, $X_f = 0.0016752$ and $R = R_{min} = 3.63/X_f$. To fit two data points we select a $k[\ ]$- function with two constants

$$k[\sigma - g] = A\exp[-B|\sigma - g|^{1/4}]$$

where $A = 1.4354477 \times 10^{20}\,s$ and $B = 25.424278$ Ksi$^{-1/4}$.

(4) Parameters corresponding to Models III and IV and to $K[\ ]$ in eqn (7).

$d_0 = 200$ $\quad c_0 = 76.778\,d_0$ $\quad A_0 = \exp[K_0/K_1]/K_2$ $\quad B_0 = K_1$

Model III $\quad K_0 = 0.0539883$ $\quad K_1 = 0.0022286$ $\quad K_2 = 1$ s

Model IV $\quad K_0 = 0.0539595$ $\quad K_1 = 0.0022286$ $\quad K_2 = 1$ s.